engineering proceedings

MDPI

Proceeding Paper

Effect of Annealing Temperature on the Microstructure, Mechanical Properties, and Electrical Conductivity of 4xxx Series Al-Based Alloys †

Mohammad Khoshghadam-Pireyousefan [1,*], Mousa Javidani [1], Alexandre Maltais [2], Julie Lévesque [3] and X.-Grant Chen [1]

[1] Department of Applied Science, University of Québec at Chicoutimi, Saguenay, QC G7H 2B1, Canada; mjavidan@uqac.ca (M.J.); xgchen@uqac.ca (X.-G.C.)
[2] Arvida Research and Development Center, Rio Tinto Aluminum, Saguenay, QC G7S 4K8, Canada; alexandre.maltais@riotinto.com
[3] Québec Metallurgy Centre, Trois-Rivières, QC G9A 5E1, Canada; julie.levesque@cegeptr.qc.ca
* Correspondence: mkpireyous@etu.uqac.ca
† Presented at the 15th International Aluminium Conference, Québec, QC, Canada, 11–13 October 2023.

Abstract: This study investigated the effects of annealing on the microstructure, mechanical properties, and electrical conductivity (EC) of AA4043 rods produced through the Properzi CCR process. Annealing was conducted at two temperatures (200 °C and 300 °C) for 4 h. Characterization techniques were performed on the rod samples, including optical microscopy, EBSD, microhardness, tensile tests, and EC measurements. The results showed a significant improvement in EC with decreased mechanical strength during annealing. The sample annealed at 300 °C exhibited the most favorable combination of EC (57.48% IACS), microhardness (41 HV), and ultimate tensile strength (124 MPa). Furthermore, the image analysis revealed slight alterations in the shape factors of eutectic Si particles with increasing annealing temperature. In addition, EBSD results demonstrated that the annealing promoted the recrystallization process.

Keywords: Al-Si conductor alloys; annealing; electrical conductivity; mechanical properties

Citation: Khoshghadam-Pireyousefan, M.; Javidani, M.; Maltais, A.; Lévesque, J.; Chen, X.-G. Effect of Annealing Temperature on the Microstructure, Mechanical Properties, and Electrical Conductivity of 4xxx Series Al-Based Alloys. *Eng. Proc.* **2023**, *43*, 14. https://doi.org/10.3390/engproc2023043014

Academic Editor: Houshang Alamdari

Published: 13 September 2023

1. Introduction

The growing global demand for electricity and the increasing adoption of renewable energy sources, such as solar and wind power, present significant challenges in their seamless integration into the electrical power grid. One of the primary obstacles involves the development of new transmission and distribution lines that can efficiently transport energy from remote farms to areas with high demand. Consequently, these high-voltage transmission lines play a pivotal role in the efficient distribution of renewable energy [1]. Two common types of aluminum conductor cables are typically employed for overhead transmission lines: aluminum conductor steel reinforced (ACSR) and all-aluminum alloy conductor (AAAC) [2]. The high density of the core steel and low strength of AA1350 cables in ACSR lines negatively affect the power transmission. Consequently, lines become heavier and are subjected to significant mechanical stresses, which ultimately pose a risk of instability. On the other hand, the AAAC cables, made of the precipitation-hardened AA6201 alloy [3–5], suffer from reduced EC (52.5% IACS) [6]. Hence, there is an increasing demand for innovative Al-based conductor cables that can provide both high strength and electrical conductivity, effectively meeting the increasing requirements of the electrical conductor industry.

Hypoeutectic Al-Si alloys (e.g., AA4043 with 5 wt.% Si) have been extensively used in the automotive industry as filler materials for welding and brazing wires. Despite their advantageous attributes, including a high strength-to-weight ratio, high castability, and excellent thermal conductivity, these alloys fall short in EC, limiting their use as electrical conductors [7]. The primary contributor to their reduced EC is the presence of coarse lamellar-like eutectic Si, which causes electron scattering, and the semiconductor Si, possessing lower intrinsic EC than Al. Additionally, impurities such as transition metals (TMs) in the solid-solution state increase the lattice distortion of Al, further diminishing the EC of the alloy.

Researchers have tackled these challenges using various approaches. These approaches involve purifying the Al matrix through Boron treatment [8], modifying the morphology of the eutectic Si by employing modifiers like Sr, and utilizing high-temperature heat treatment [9–13]. Another potential strategy to enhance the EC of these alloys is the application of plastic deformation to achieve a homogeneous dispersion of refined eutectic Si within the Al matrix [14]. Guo et al. [13] studied the impact of Sr and Sb elemental modification and T6 heat treatment on the EC of Al-8Si alloy. The results revealed that Sr modification led to a transformation of the eutectic Si morphology into a fibrous shape, which significantly improved EC. In contrast, the influence of the Sb modifier was comparatively weaker. Additionally, the T6 treatment was found to increase EC by spheroidization of flake-like eutectic Si. However, prolonged treatment negatively affected EC due to the coarsening of fibrous eutectic structures.

Ye et al. [14] conducted a study to examine the impact of hybrid boron treatment, Sr modification, homogenization heat treatment, and hot extrusion on the EC and ultimate tensile strength (UTS) of Al-4Si alloy. The results indicated that the incorporation of Sr-B treatment led to an increase in EC from 41.8% IACS to 46.6% IACS. After the high-temperature solution treatment, the EC increased to 53.9% IACS. The EC was further enhanced to 57.3% IACS after the hot extrusion process. Compared to the as-cast condition, the EC, UTS, and elongation after the treatments were enhanced by 41.6%, 60.9%, and 136.3%, respectively. All the aforementioned treatments can be achieved using the Properzi continuous casting-rolling (CCR) process, which is widely employed for the production of Al conductor cables. This process entails casting a trapezoidal cross-section bar using a Properzi wheel, followed by hot rolling in an in-line multi-stand process to produce a rod with a diameter of 9.5 mm. The hot rolling process involves applying up to a 90% reduction in the area [15–17].

Despite extensive research studies on the mechanical properties of hypoeutectic Al-Si products, the effect of low-temperature direct annealing on the EC of these materials has never been reported. This study investigates the impact of direct annealing at two temperatures (200 and 300 °C) on the mechanical properties, EC, and microstructure of the AA4043 alloy produced by the Properzi CCR process.

2. Materials and Methods

The AA4043 rods were manufactured using the Properzi CCR process, as depicted in Figure 1. After preparing the liquid metal with the targeted chemical composition in the melting furnace, the molten metal underwent degassing, grain refinement, B treatment, and Sr modification. The chemical composition of the prepared metal, analyzed by optical emission spectroscopy, is presented in Table 1. All chemical compositions are presented in weight percent (wt.%). The liquid metal was cast by the Properzi casting machine, through which the trapezoidal cross-section bar was produced. Subsequently, the cast bar was fed into an in-line multiple stand hot rolling unit, where the bar was deformed into the 9.5 mm diameter rod. The as-rolled rods (referred to as the As-R sample) were sectioned and subjected to annealing at 200 °C and 300 °C for 4 h. These annealed samples are called the 4–200 and 4–300 samples. The annealing process was conducted using a programmable furnace without prior solution heat treatment. Following annealing, the samples were cooled gradually inside the furnace until they reached room temperature.

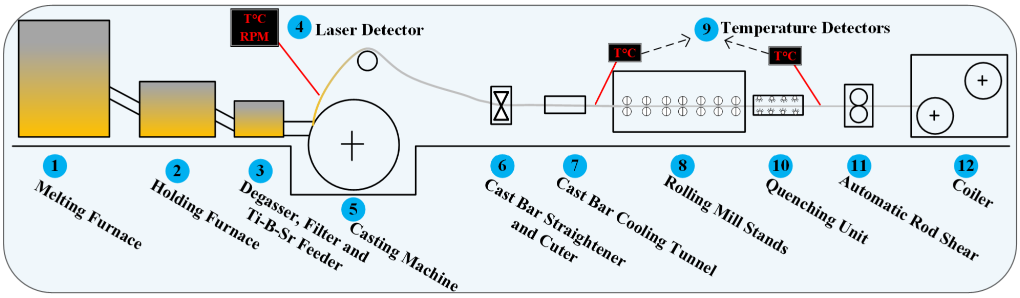

Figure 1. Flowchart of Properzi continuous casting-rolling for rod production.

Table 1. The chemical composition of the AA4043 rods studied (wt.%).

Alloy	Elements								
	Si	**Fe**	**Cu**	**Mg**	**Ti**	**V**	**B**	**Sr**	**Al**
AA4043	4.9	0.10	0.03	0.001	0.008	0.001	0.004	0.029	Bal.

The metallographic samples were prepared following the standard grinding and polishing procedures. The as-polished samples were examined using optical microscopy (Nikon, Eclipse ME600, Nikon Co, Tokyo, Japan). The characteristics of the eutectic Si particles were analyzed on optical micrographs obtained from the As-R and annealed samples. For each sample, measurements were conducted by ImageJ software (version 1.53t) on 20 micrographs, through which the mean aspect ratio, mean equivalent circular diameter, and mean sphericity of the eutectic Si particles were quantified. Additionally, scanning electron microscopy (SEM, JEOL-6480LV, JEOL Ltd., Tokyo, Japan) equipped with an electron backscatter diffraction (EBSD) system was employed to investigate the deformed structure of the rods in longitudinal sections. The EBSD analysis was conducted with a step size of 1 µm. The EBSD raw data was then analyzed using Channel 5 and ATEX [18] software. For the analysis of the grain microstructure, the misorientation angles were categorized into three ranges: 2–5° for low-angle grain boundaries (LAGBs), 5–15° for medium-angle grain boundaries (MAGBs), and greater than 15° for high-angle grain boundaries (HAGBs).

Microhardness and tensile tests were conducted to assess the mechanical properties of the rods. For microhardness testing, longitudinal sections of the samples were examined parallel to the rolling direction of the rod. A force of 25 g was applied with a dwell time of 20 s. At least eight measurements were taken, and the average hardness value was recorded. Tensile tests were performed on the rod samples with a gauge length of 250 mm and a diameter of 9.5 mm, following the ASTM B557M standard [19]. The average strength values were determined by three tensile tests for each condition. The EC was measured using a Megger DLRO10HD resistance ohmmeter (Megger, Dallas, TX, USA) on the rod samples of 300 mm in length and 9.5 mm in diameter, following the ASTM B193 standard [20]. At least five measurements were taken for each sample, and the average EC value was reported.

3. Results and Discussion

3.1. Mechanical Properties and Electrical Conductivity

Figure 2a illustrates the impact of annealing states (e.g., As-R, 4-200, and 4-300) on the microhardness and EC of the studied samples. As the annealing temperature increased, the EC value significantly improved while microhardness decreased. The As-R sample had the lowest EC value of 50.08% IACS. However, the 4-200 and 4-300 samples exhibited enhanced EC values of 54.18% IACS and 57.48% IACS, respectively. The As-R sample had the highest microhardness value of 48 HV, while the 4-300 sample displayed the lowest value of 41 HV.

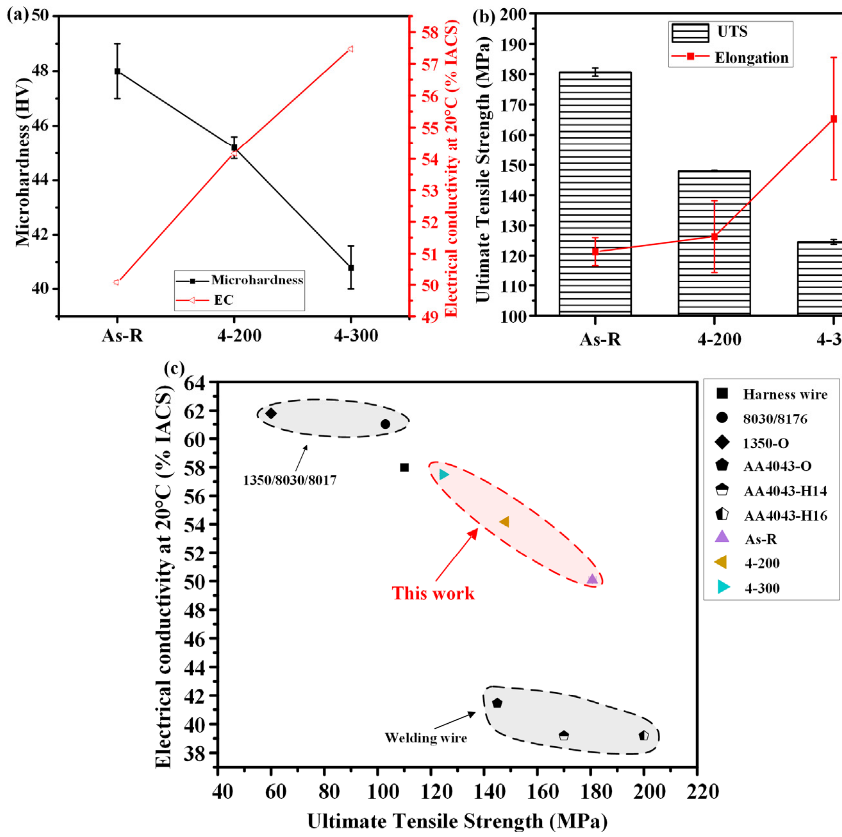

Figure 2. Influence of annealing temperature on (**a**) EC and microhardness (**b**) Ultimate tensile strength and elongation of AA4043 alloy, and (**c**) comparison of UTS and EC of this study with commercial Al alloys including harness wire [21], AA8030/AA8176 [22], AA1350-O [23], AA4043-(O, H14, and H16) welding wire (from MatWeb Material Property Database).

Figure 2b shows the UTS and elongation for As-R and annealed samples. The UTS values decreased with increasing annealing temperature, whereas the elongation of the samples increased. The UTS values exhibited a similar trend with microhardness. The As-R sample exhibited a UTS of 180 MPa, while the 4-200 sample showed a UTS of 148 MPa, and the 4-300 sample displayed a further decrease to 124 MPa. In terms of elongation, the As-R sample had a value of 18%, which slightly increased to 18.6% for the 4-200 sample and further increased to 22.5% for the 4-300 sample.

Figure 2c compares the EC and UTS values of the samples from this study, the AA4043 welding wire, and the automobile harness wires (e.g., AA1350-O, AA8030, and AA8017 alloys). The comparison provides insights into the relative performance and suitability of these materials for electrical conductor applications based on their EC and UTS properties. The As-R sample exhibited higher EC and UTS values than conventional AA4043 welding wires. The approximate 10% IACS improvement in the EC of the As-R sample compared to traditional AA4043 welding wires signifies the effectiveness of the B-treatment and Sr-modification processes in this study. Moreover, a comparison between the 4-300 and As-R samples indicated an additional 8% IACS improvement in EC due to the annealing treatment. Therefore, a significant improvement in the EC is achieved in this study, approximately 40% (from 41% IACS of welding wires to 57.48% IACS of 4-300 samples). The findings of this study suggest that the employed production techniques and treatments have effectively enhanced the EC of AA4043, showing its potential as a promising candidate for various electrical conductor applications, such as electrical wiring, power transmission, and other related applications.

3.2. Morphology of Eutectic Si Particles

The morphology and distribution of eutectic Si particles play a crucial role in determining the EC and mechanical properties of hypoeutectic Al-Si alloys. Figure 3 presents the typical optical micrographs of the As-R and annealed samples in the longitudinal section, with eutectic Si particles appearing grey (indicated by red arrows). As depicted in Figure 3a–c, the eutectic Si particles exhibited a homogeneous distribution with a fine globular morphology along the rolling direction (RD), indicating the effectiveness of Sr modification and the severe plastic deformation induced by the Properzi CCR process.

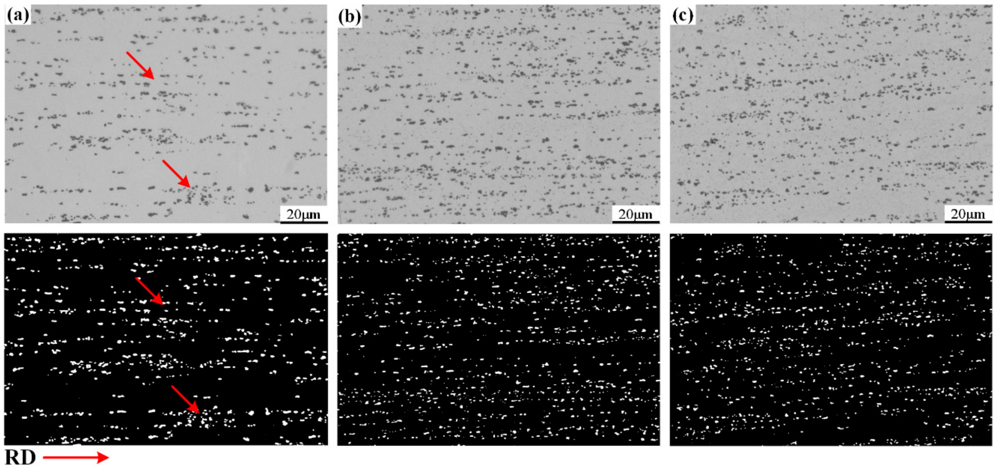

Figure 3. OM (upper micrographs) and image analysis (bottom micrographs) from ImageJ software of (**a**) As-R, (**b**) 4-200, and (**c**) 4-300 samples. RD stands for the rolling direction.

The effect of annealing on the morphology of the Si particles was investigated through statistical analysis using image analysis, as presented in Figure 4. The mean equivalent circular diameters of the eutectic Si particles decreased as a function of annealing temperature (Figure 4a). For instance, it decreased from 1.05 μm in the As-R sample to 0.91 μm and 0.86 μm in the 4-200 and 4-300 samples, respectively. Similarly, Figure 4b demonstrates that the mean aspect ratio of the eutectic Si particles followed a similar trend, decreasing from approximately 1.8 in the As-R sample to around 1.6 in both annealed conditions.

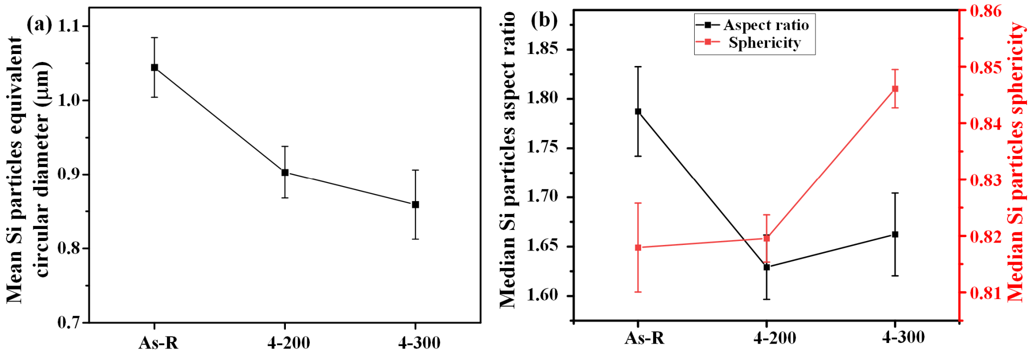

Figure 4. Morphological features of eutectic Si as a function of annealing temperature: (**a**) mean equivalent circular diameter, (**b**) mean aspect ratio and sphericity.

The spherical morphology of eutectic Si particles offers the advantage of providing the smallest interface with the α-Al matrix compared to other Si morphologies. This decreases the matrix/precipitate interface, which contributes to the electron scattering, thus longer access paths for free electron traveling between eutectic Si particles, leading to improved EC [9,24]. Sphericity, which quantifies the similarity of a particle to a sphere, is an important parameter in assessing the shape of particles. A sphericity value of 1 indicates a perfectly spherical shape. Figure 4b presents the sphericity values for the As-R and annealed samples. The sphericity value assigned to the As-R sample is 0.82, indicating that it achieves up to 82% of the maximum possible sphericity. These results indicate that Sr modification and the Properzi CCR production method were quite effective in producing AA4043 Al alloys with eutectic Si particles exhibiting a near-perfect spherical shape. Furthermore, Figure 4b demonstrates a slight enhancement in sphericity of the 4-200 sample, showing an increase from 0.82 to 0.83 and further improvements to 0.85 for the 4-300 sample.

The quantitative analysis showed that increasing the annealing temperature led to changes in the morphology of eutectic Si. However, such changes in eutectic Si morphology were not substantial, and therefore, its influence on the EC may be negligible. This finding differs from previous studies in the literature [9,12,25], which have shown significant improvements in EC through eutectic Si modification using high-temperature heat treatments, typically ranging from 500 °C to 540 °C.

3.3. Microstructural Evolution

Figure 5a–c presents the inverse pole figure (IPF) maps at the longitudinal section for the As-R sample and samples annealed at 200 °C and 300 °C for 4 h. From Figure 5a, it can be observed that the majority of the grains in the As-R sample exhibit elongated features aligned with the rolling direction. Similarly, even after annealing at 200 °C and 300 °C for 4 h, as shown in Figure 5b,c, the grains maintain their elongated shape in the rolling direction.

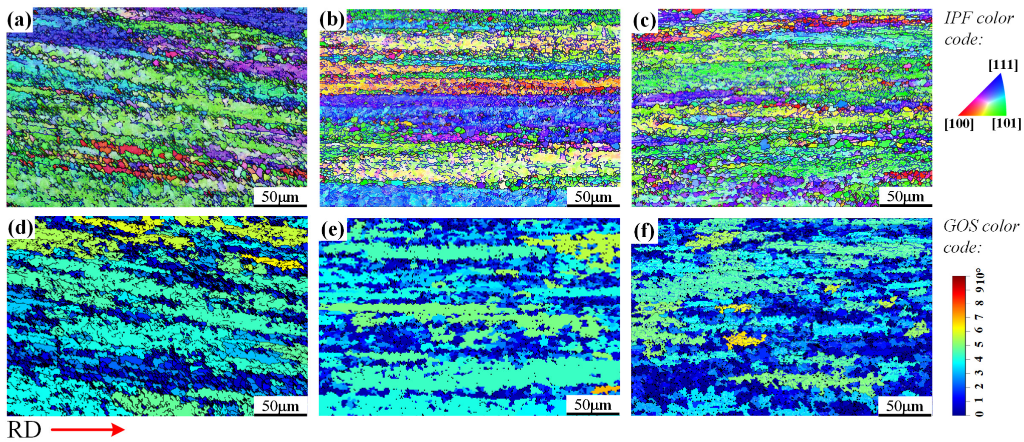

Figure 5. IPF and GOS maps of As-R (**a**,**d**), 4-200 (**b**,**e**), and 4-300 (**c**,**f**) samples, respectively.

Figure 6 shows the quantitative results of misorientation angles as a function of annealing temperature. The results indicate that the fraction of LAGBs decreases while the fractions of MAGBs and HAGBs increase in the 4-200 and 4-300 annealed samples compared to the As-R sample. Specifically, the sample annealed at a lower temperature (4-200) exhibits the highest fraction of MAGBs, while the sample annealed at a higher temperature (4-300) has the lowest fraction. MAGBs are considered to be the transitional boundaries between LAGBs and HAGBs. The results confirm a higher rate of transformation of LAGBs into MAGBs and HAGBs in the high-temperature annealed sample, leading to a higher fraction of recrystallization. On the other hand, in the low-temperature annealed sample, MAGBs play a more significant role in softening the samples. Moreover, the higher proportion of MAGBs in the 4-200 samples supports the hypothesis that recovery is the predominant softening mechanism in lower-temperature annealed samples, while recrystallization prevails in high-temperature annealed samples, as reported in previous studies [26,27].

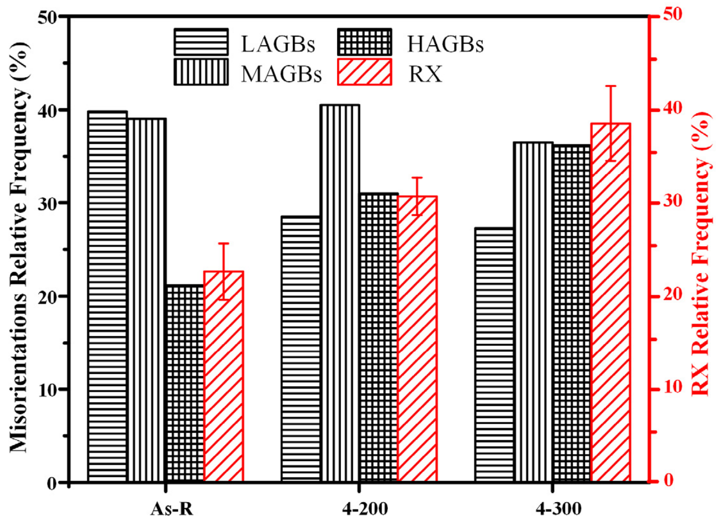

Figure 6. The effect of annealing temperature on the misorientation angle distribution and recrystallization.

The recovery and recrystallization in the annealed samples are further supported by the grain orientation spread (GOS) maps presented in Figure 5d–f for the As-R, 4-200, and 4-300 samples, respectively. The GOS maps provide insights into the dislocation density and strain distribution within each grain. Grains with GOS values below 2° are associated with recrystallized grains, while higher GOS values (>5°) indicate deformed structures [28]. In Figure 5d, the As-R sample exhibits a higher GOS value (>5°), indicating a significant proportion of deformed structure with limited recovery and recrystallization. On the other hand, the annealed samples show GOS values below 5°, confirming substantial recovery and recrystallization. The presence of subgrains within the grain interiors further supports the occurrence of recovery in the annealed samples. Additionally, small grains observed along the initial grain boundaries in the As-R and annealed samples provide further evidence of partial recrystallization [28]. Figure 6 displays the fraction of recrystallized grains as a function of annealing temperature. The As-R sample exhibits a recrystallization area fraction of 23%, which increases to 31% and 38% for the annealed samples at 4-200 and 4-300, respectively. This confirms the progressive increase in recrystallization with higher annealing temperatures.

While the observed partial recrystallization and changes in misorientation angles provide some insights into the mechanical properties (such as UTS, microhardness, and elongation), they may not fully explain the improvements in the EC observed in the annealed samples. Future study is necessary to identify the main factors that contribute to the enhanced EC resulting from direct annealing.

4. Conclusions

The effects of direct annealing on the EC, microhardness, UTS, and elongation of AA4043 rods produced using the Properzi CCR method were evaluated. The following conclusions can be drawn:

Increasing the annealing temperature led to a decrease in UTS and microhardness while simultaneously increasing elongation and EC. This indicates that the direct annealing temperature significantly influences the mechanical and electric properties of AA4043.

Among the annealed samples, the one annealed at a higher temperature (300 °C for 4 h) exhibited the highest EC (57.48% IACS), elongation (22.5%), and the lowest UTS (124 MPa) and microhardness (41 HV).

Quantitative image analysis revealed that the morphological changes of the eutectic Si particles were marginally affected by the annealing process.

EBSD analysis showed that most grains in both as-rolled and annealed samples retained their elongated shape aligned with the rolling direction. However, the annealing at 200 °C and 300 °C resulted in increased MAGBs and recrystallized grains, indicating recovery and recrystallization at elevated temperatures.

Overall, these findings provide insights into the influence of direct annealing on the properties of AA4043 and the role of annealing temperature in controlling its mechanical and electrical behavior.

Author Contributions: Conceptualization, M.J., A.M. and M.K.-P. methodology, M.K.-P. and M.J.; validation, M.J., A.M. and X.-G.C.; formal analysis, M.K.-P.; investigation, M.K.-P.; writing—original draft preparation, M.K.-P.; writing—review and editing M.J, A.M., J.L. and X.-G.C.; supervision, M.J. and X.-G.C.; project administration M.J. All authors have read and agreed to the published version of the manuscript.

Funding: This research was funded by the Natural Sciences and Engineering Research Council of Canada (NSERC) under the Grant numbers of ALLRP 576503–22, and Centre Quebecois de Recherche et de Developpement de l'Aluminium (CQRDA) under the Grant numbers of CRDPJ 514651-17.

Institutional Review Board Statement: Not applicable.

Informed Consent Statement: Not applicable.

Data Availability Statement: Not applicable.

Acknowledgments: The authors would like to acknowledge the industrial partners of the project Rio Tinto Aluminum, MindCore Technologies and CANMEC Group Inc. The authors extend their appreciation to the technical team of Rio Tinto Aluminum and Québec Metallurgy Centre for their support in preparing samples.

Conflicts of Interest: The authors declare no conflict of interest.

References

1. Bagherian, M.A.; Mehranzamir, K. A comprehensive review on renewable energy integration for combined heat and power production. *Energy Convers. Manag.* **2020**, *224*, 113454. [CrossRef]
2. Zhang, J.; Peng, J. A review on aluminum alloy conductors influenced by alloying elements and thermomechanical treatments: Microstructure and properties. *J. Mater. Res.* **2023**, *38*, 1488–1509. [CrossRef]
3. Khangholi, S.N.; Javidani, M.; Maltais, A.; Chen, X.G. Review on recent progress in Al–Mg–Si 6xxx conductor alloys. *J. Mater. Res.* **2022**, *37*, 670–691. [CrossRef]
4. Nikzad Khangholi, S.; Javidani, M.; Maltais, A.; Chen, X.-G. Optimization of mechanical properties and electrical conductivity in Al–Mg–Si 6201 alloys with different Mg/Si ratios. *J. Mater. Res.* **2020**, *35*, 2765–2776. [CrossRef]
5. Khangholi, S.N.; Javidani, M.; Maltais, A.; Chen, X.G. Effects of natural aging and pre-aging on the strength and electrical conductivity in Al-Mg-Si AA6201 conductor alloys. *Mater. Sci. Eng. A* **2021**, *820*, 141538. [CrossRef]
6. Khangholi, S.N.; Javidani, M.; Maltais, A.; Chen, X.-G. Effect of Ag and Cu addition on the strength and electrical conductivity of Al-Mg-Si alloys using conventional and modified thermomechanical treatments. *J. Alloys Compd.* **2022**, *914*, 165242. [CrossRef]
7. Ganesh, M.R.S.; Reghunath, N.J.; Levin, M.; Prasad, A.; Doondi, S.; Shankar, K.V. Strontium in Al–Si–Mg Alloy: A Review. *Met. Mater. Int.* **2022**, *28*, 1–40. [CrossRef]
8. Cui, X.; Cui, H.; Wu, Y.; Liu, X. The improvement of electrical conductivity of hypoeutectic Al-Si alloys achieved by composite melt treatment. *J. Alloys Compd.* **2019**, *788*, 1322–1328. [CrossRef]
9. Li, K.; Zhang, J.; Chen, X.; Yin, Y.; He, Y.; Zhou, Z.; Guan, R. Microstructure evolution of eutectic Si in Al-7Si binary alloy by heat treatment and its effect on enhancing thermal conductivity. *J. Mater. Res. Technol.* **2020**, *9*, 8780–8786. [CrossRef]
10. Mulazimoglu, M.H.; Drew, R.A.L.; Gruzleski, J.E. The electrical conductivity of cast Al−Si alloys in the range 2 to 12.6 wt pct silicon. *Metall. Trans. A* **1989**, *20*, 383–389. [CrossRef]
11. Mulazimoglu, M.H.; Drew, R.A.L.; Gruzleski, J.E. The effect of strontium on the electrical resistivity and conductivity of aluminum-silicon alloys. *Metall. Trans. A* **1991**, *18*, 941–947. [CrossRef]
12. Mulazimoglu, M.H.; Drew, R.A.L.; Gruzleski, J.E. Solution Treatment Study of Cast Al–Si Alloys by Electrical Conductivity. *Can. Metall. Q.* **1989**, *28*, 251–258. [CrossRef]
13. Guo, J.; Guan, Z.-P.; Yan, R.-F.; Ma, P.-K.; Wang, M.-H.; Zhao, P.; Wang, J.-G. Effect of Modification with Different Contents of Sb and Sr on the Thermal Conductivity of Hypoeutectic Al-Si Alloy. *Metals* **2020**, *10*, 1637. [CrossRef]
14. Ye, H.; Cui, X.; Li, X.; Cui, H.; Zhang, B.; Li, H.; Pan, Y.; Feng, R.; Wu, Y.; Liu, X. Fabrication of hypoeutectic Al-4Si alloy with high electrical conductivity, high plasticity and medium strength by the dual treatment of Al matrix and eutectic Si microstructure. *J. Alloys Compd.* **2021**, *885*, 161117. [CrossRef]
15. Marcantoni, G.E. From Molten Metal to 3.2 mm Wire for Mechanical Applications. In *Light Metals 2012*; John Wiley & Sons, Inc.: Hoboken, NJ, USA, 2012; pp. 251–255.

16. Lewis, D.M. The production of non-ferrous metal slab and bar by continuous-casting and rolling methods. *Metall. Rev.* **1961**, *6*, 143–192. [CrossRef]
17. Stefanescu, D.M.; Davis, J.R.; Destefani, J.D. Metals Handbook, Vol. 15—Casting. *ASM Int.* **2008**, *15*, 937.
18. Beausir, B.; Fundenberger, J.-J. Analysis Tools for Electron and X-ray Diffraction, ATEX–Software, Université de Lorraine-Metz. 2017. Available online: www.atex-software.eu (accessed on 10 July 2023).
19. *ASTM B557M*; Standard Test Methods for Tension Testing Wrought and Cast Aluminum- and Magnesium-Alloy Products. ASTM: West Conshohocken, PA, USA, 2023.
20. *ASTM B193*; Standard Test Method for Resistivity of Electrical Conductor Materials. ASTM: West Conshohocken, PA, USA, 2020. [CrossRef]
21. *ISO 6722-2*; Road Vehicles—60 V and 600 V Single-Core Cables—Part 2: Dimensions, Test Methods and Requirements for Aluminium Conductor Cables. ISO: Geneva, Switzerland, 2019.
22. *ASTM B800*; Standard Specification for 8000 Series Aluminum Alloy Wire for Electrical Purposes-Annealed and Intermediate Tempers. ASTM: West Conshohocken, PA, USA, 2021. [CrossRef]
23. *ASTM B609/B609M*; International: Standard Specification for Aluminum 1350 Round Wire, Annealed and Intermediate Tempers, for Electrical Purposes. ASTM: West Conshohocken, PA, USA,, 2021. [CrossRef]
24. Toberer, E.S.; Baranowski, L.L.; Dames, C. Advances in Thermal Conductivity. *Annu. Rev. Mater. Res.* **2012**, *42*, 179–209. [CrossRef]
25. Vandersluis, E.; Ravindran, C.; Bamberger, M. The Detriment of Coherency Strains to the Electrical Conductivity of Naturally-Aged B319 Al Alloy. *Metall. Mater. Trans. A Phys. Metall. Mater. Sci.* **2020**, *51*, 5923–5931. [CrossRef]
26. Wang, M.J.; Sun, C.Y.; Fu, M.W.; Liu, Z.L.; Qian, L.Y. Study on the dynamic recrystallization mechanisms of Inconel 740 superalloy during hot deformation. *J. Alloys Compd.* **2020**, *820*, 153325. [CrossRef]
27. Yuan, L.; Gou, F.; Sun, D.; Li, Z.; Xue, Y. The Effects of Cold Rolling and Annealing on the Microstructure Evolution of Ordered C-2000 Alloy during Metallic Wire Preparation. *Metals* **2023**, *13*, 651. [CrossRef]
28. Mofarrehi, M.; Javidani, M.; Chen, X.G. Effect of Mn content on the hot deformation behavior and microstructure evolution of Al–Mg–Mn 5xxx alloys. *Mater. Sci. Eng. A* **2022**, *845*, 143217. [CrossRef]